RAPPORTSERIE

Nr. 15 - Oslo 1984

TORGNY E. VINJE:

Frequency distribution of sea ice, ridges, and water openings in the Greenland and Barents Seas. - A preliminary report on the 'Birds Eye' observations.

NORSK POLARINSTITUTT

Nr. 15 - Oslo 1984

TORGNY E. VINJE:

Frequency distribution of sea ice, ridges, and water openings in the Greenland and Barents Seas. - A preliminary report on the 'Birds Eye' observations.

Contents

1. Introduction

There are three major areas in the Atlantic sector of the Arctic with different sea ice characteristics. These are the East Greenland Current, the Jan Mayen Gyre, and the Barents Sea.

The East Greenland Current (Fig. 1) is a continuation of the Transpolar Current originating north of Siberia. This cold polar current carries multi-year drift ice with an average thickness of 4 - 5 m. Between 2 and 15 km^3 of ice passes through the Fram Strait per day (Vinje 1976). This is without comparison the greatest ice stream on earth. A considerable acceleration takes place when the drift ice passes through the Fram Strait, and during the cold season this creates temporary water openings which readily freeze over. The ice in the East Greenland Current therefore consists of a mixture of multi-year and first year ice of variable thickness.

The Jan Mayen Gyre is a mixing area for the warmer water from the Norwegian Sea and the colder water from the Greenland Sea. The surface circulation during the winter and spring seasons is generally reflected very

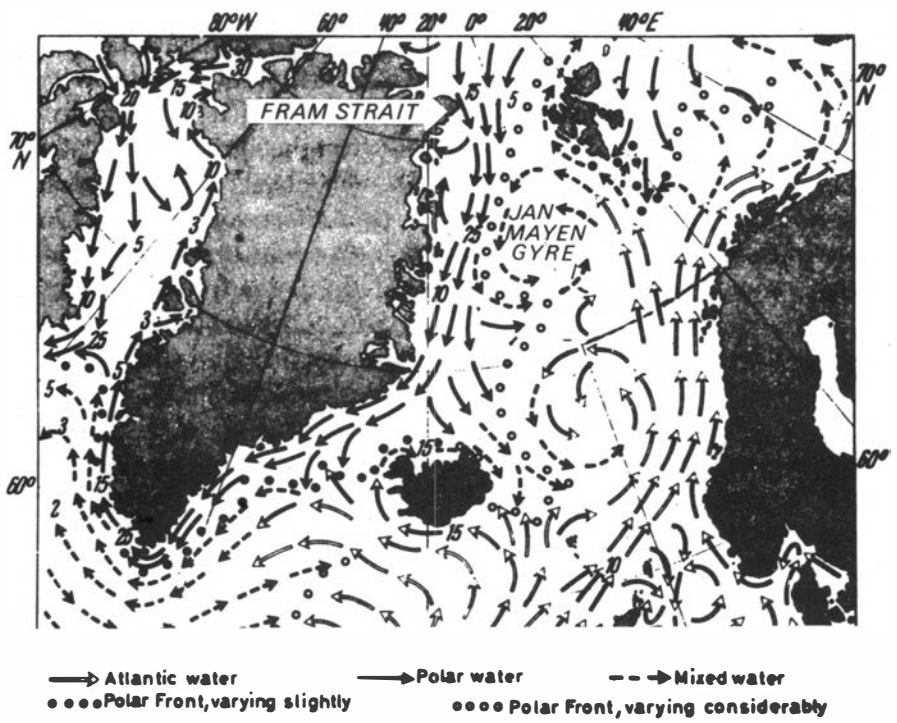

Fig. 1. Surface currents and distribution of polar and Atlantic water in the Greenland, Norwegian, and Barents Seas (after G. Dietrich: General Oceanography. An Introduction, Interscience Publisher. 1963).

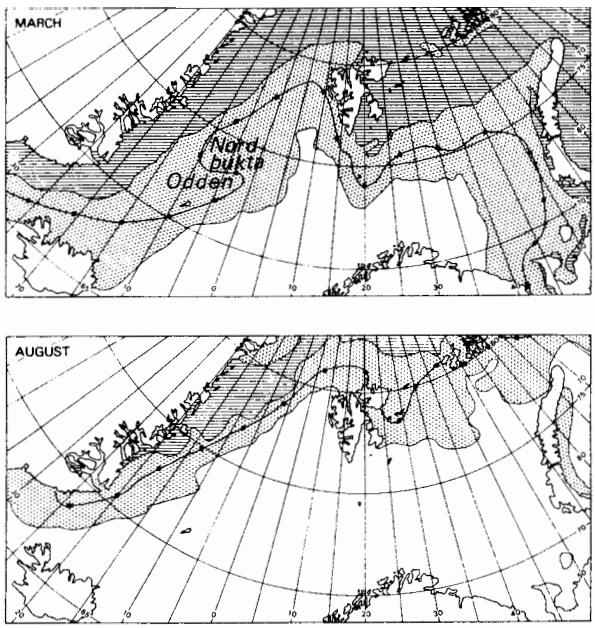

Fig. 2. Borders of maximum and minimum extension of 4/10 or more of sea ice for March and August, 1966-1975. The central curve shows the median border (Vinje 1976).

clearly in the distribution of sea ice in the area. The sea ice features Odden and Nordbukta (Fig. 2) were named so by sealers from the time they started hunting in this area in 1850. The sea ice in Odden consists mainly of locally formed ice. Sometimes it may be blown away by strong winds, otherwise it is disintegrated locally. The sea temperature in Nordbukta is generally higher than in Odden and the formation of new ice correspondingly less frequent.

In the Barents Sea the drift ice is generally formed locally. However, the outflow of ice from the Arctic Ocean through the passages east of Svalbard may be of considerable magnitude for shorter periods (Loeng & Vinje 1979), and some of the ice in the eastern part of the Svalbard archipelago does not always melt during the summer. The composition of the sea ice in the Barents Sea may therefore be quite complex, consisting of multi-year, thick winter-, and new ice produced locally, as well as the same types imported from the Arctic Ocean.

2. Distribution of sea ice

During the cold season the southern border of the sea ice in the Atlantic sector is determined mainly by the distribution of cold and warm currents. The deviation from the mean atmospheric circulation causes the more short-lived as well as the interannual deviation of the sea ice distribution from its mean. A comparison between Figs. 1 and 2 shows this accordance between the prevailing currents and the undulating sea ice edge during the cold season.

The conditions are somewhat different during the ablation period, when radiation plays the dominant role by its heating of the surface water which again melts the ice. Direct melting of the ice by the sun will also increase as the snow gets wetter and more water-soaked. The saltier and

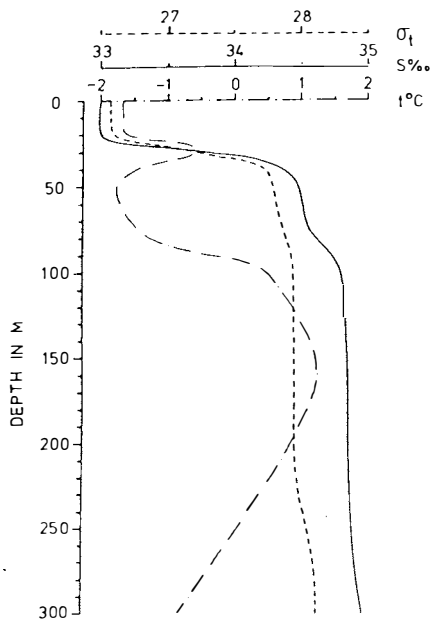

Fig. 3. Typical vertical profile of the water masses in the northern part of the Barents Sea. The maximum temperature is observed below 100 m (Loeng & Vinje 1979).

heavier warmer water (Fig. 3) submerges the less saline and lighter polar water and will generally not be in direct contact with the ice north of the oceanic polar front. The disintegration of the sea ice is therefore mainly caused by meteorological factors, particularly radiation, turbulent transfer of heat, wind drift and wave effects. The interannual variation of the sea ice extension is considerable (Fig. 2), which reflects the high variability of the combined meteorological and oceanographic effects.

2.1. Monthly frequency distribution

The distribution of the average sea ice concentration for the 25-year period 1953-1977 (Fig. 4) is based on a digitized set of data observations of sea ice, atmospheric pressure and temperature. This data set was kindly provided by Dr. J. E. Walsh, National Center of Atmospheric Research, Boulder, Colorado, and includes the whole Arctic. Each number on Fig. 4 represents the 25 years average sea ice cover at the end of each month, given in tenths within a square of 60 x 60 nautical miles. The intervals are: $1/10 \leqslant 1 < 2/10$, $2/10 \leqslant 2 < 3/10$, etc. The maximum southern sea ice extension is found at the end of March and shows that no ice has been observed south of 73°N in the western part of the Barents Sea (west of 40°E). This is in fair agreement with observations for the period 1966-1975 (Vinje 1976) with regard to latitude. The latter observations indicate, however, a maximum western limit at about 37°E instead of 40°E. At the end of July, August, and September, no ice has been observed in the Barents Sea south of 75°N, and for August and September the southern maximum extension is 77°N during the 25-year period. There is a clear difference in concentration north and south of 80°N during the warm season. To the north the sea ice concentration is generally fairly high while south of this latitude we always have on

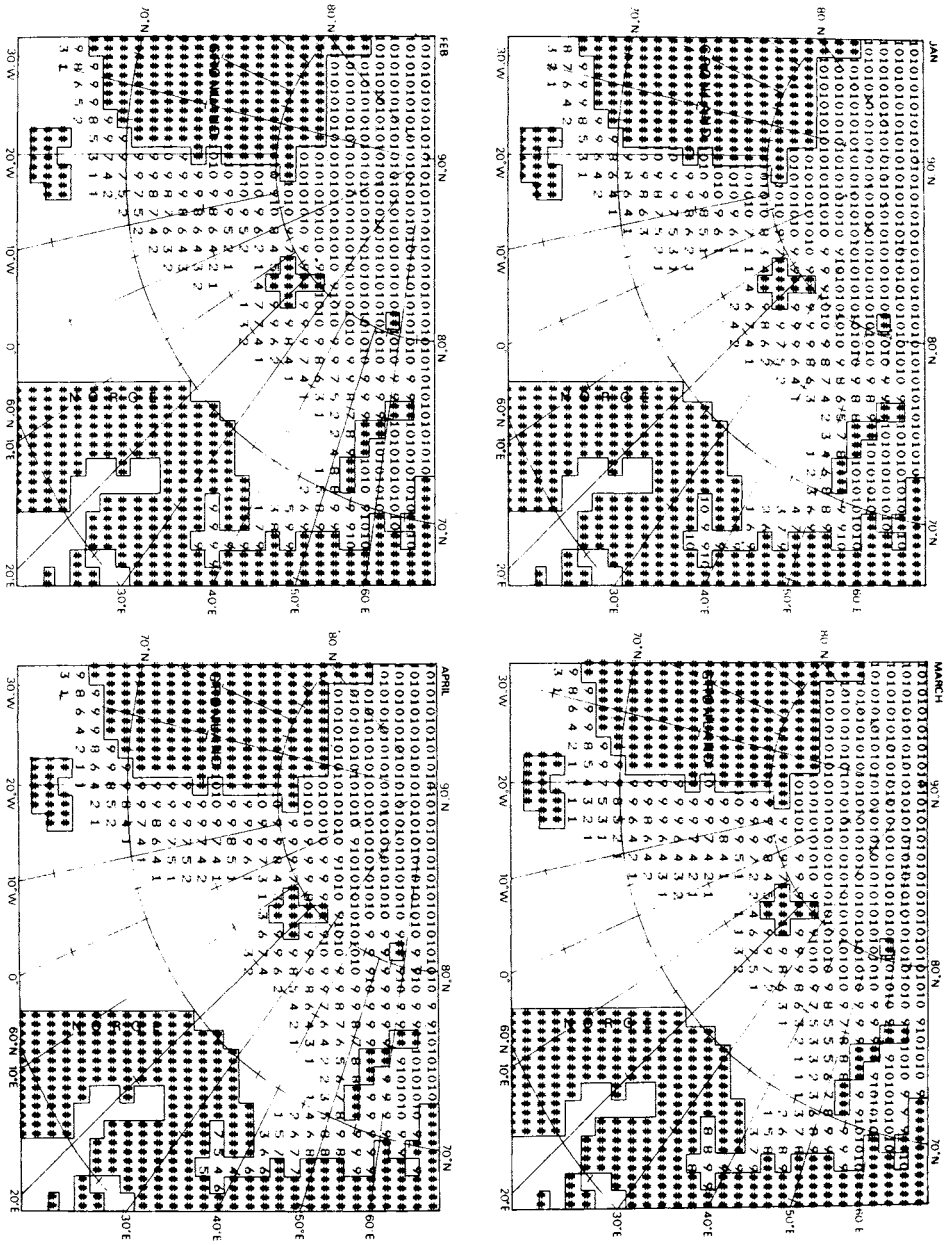

Fig. 4. Average sea ice cover at the end of each month for the period 1953-1977. The coverage is given in tenths within squares of 60 x 60 nautical miles. The intervals are: $1/10 \leqslant 1 < 2/10$, $2/10 \leqslant 2 < 3/10$, etc. The data have kindly been provided by Dr. J. E. Walsh, NCAR, Boulder, Colorado.

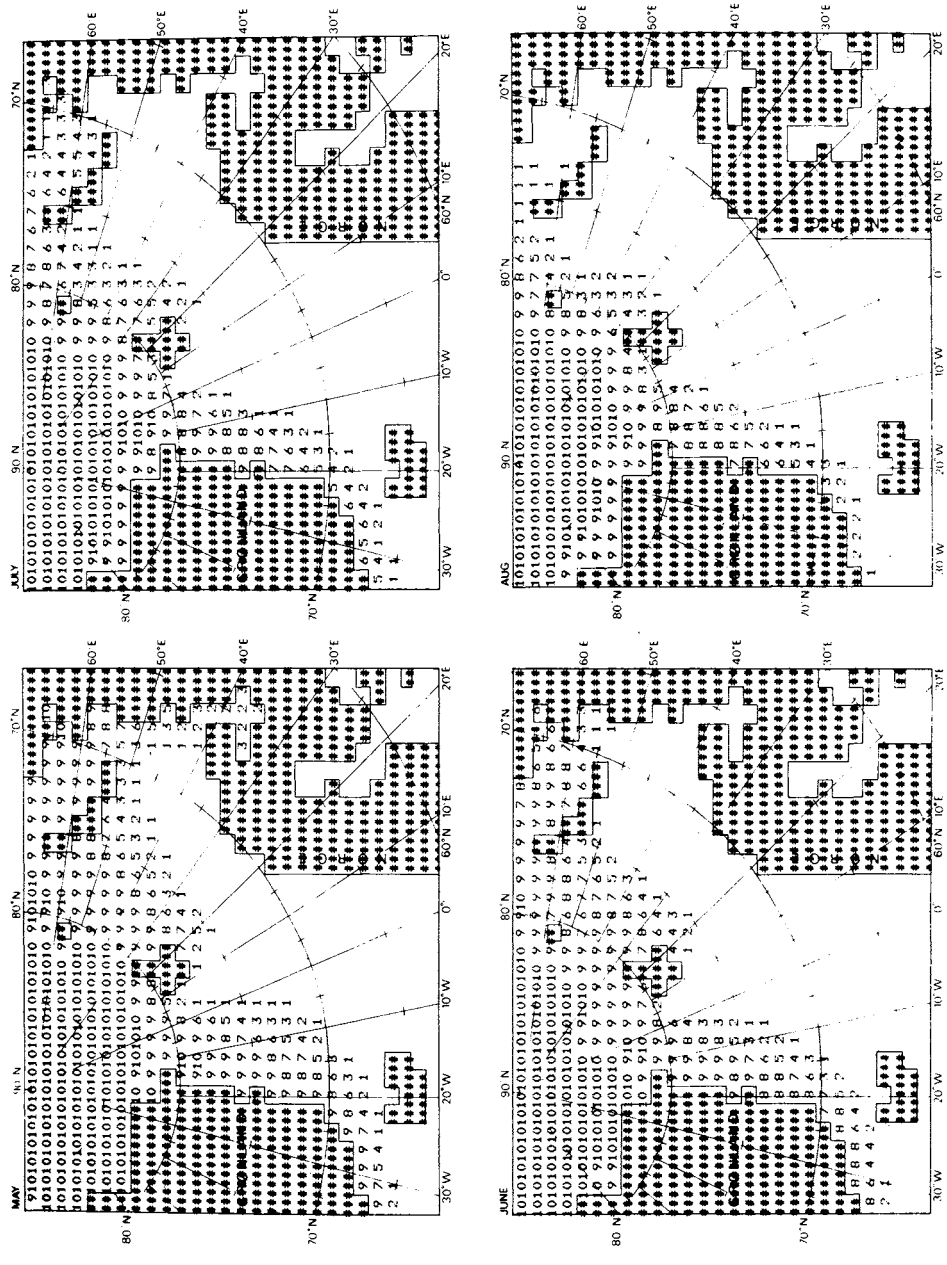

Fig. 4. Continued.....

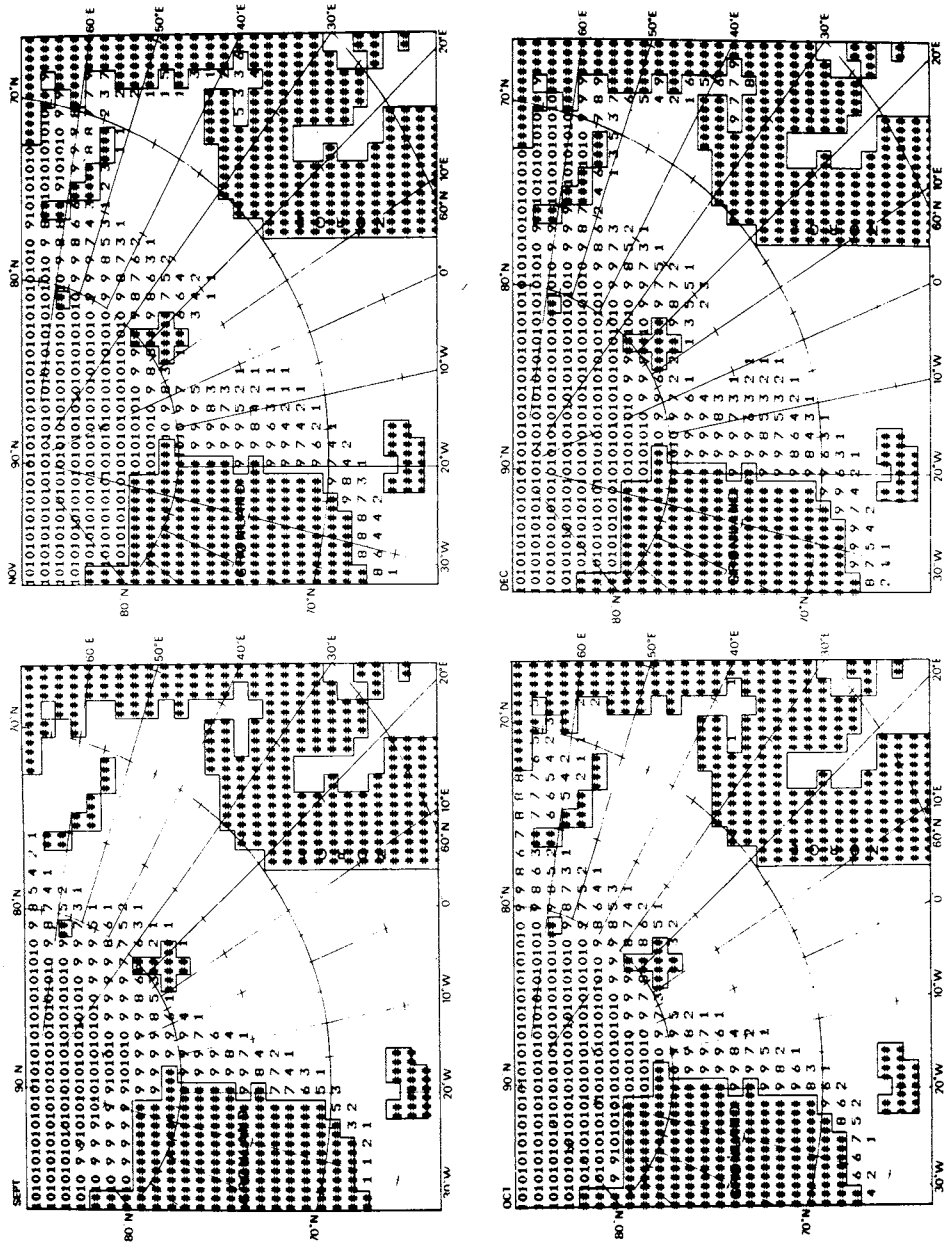

Fig. 4. Continued.....

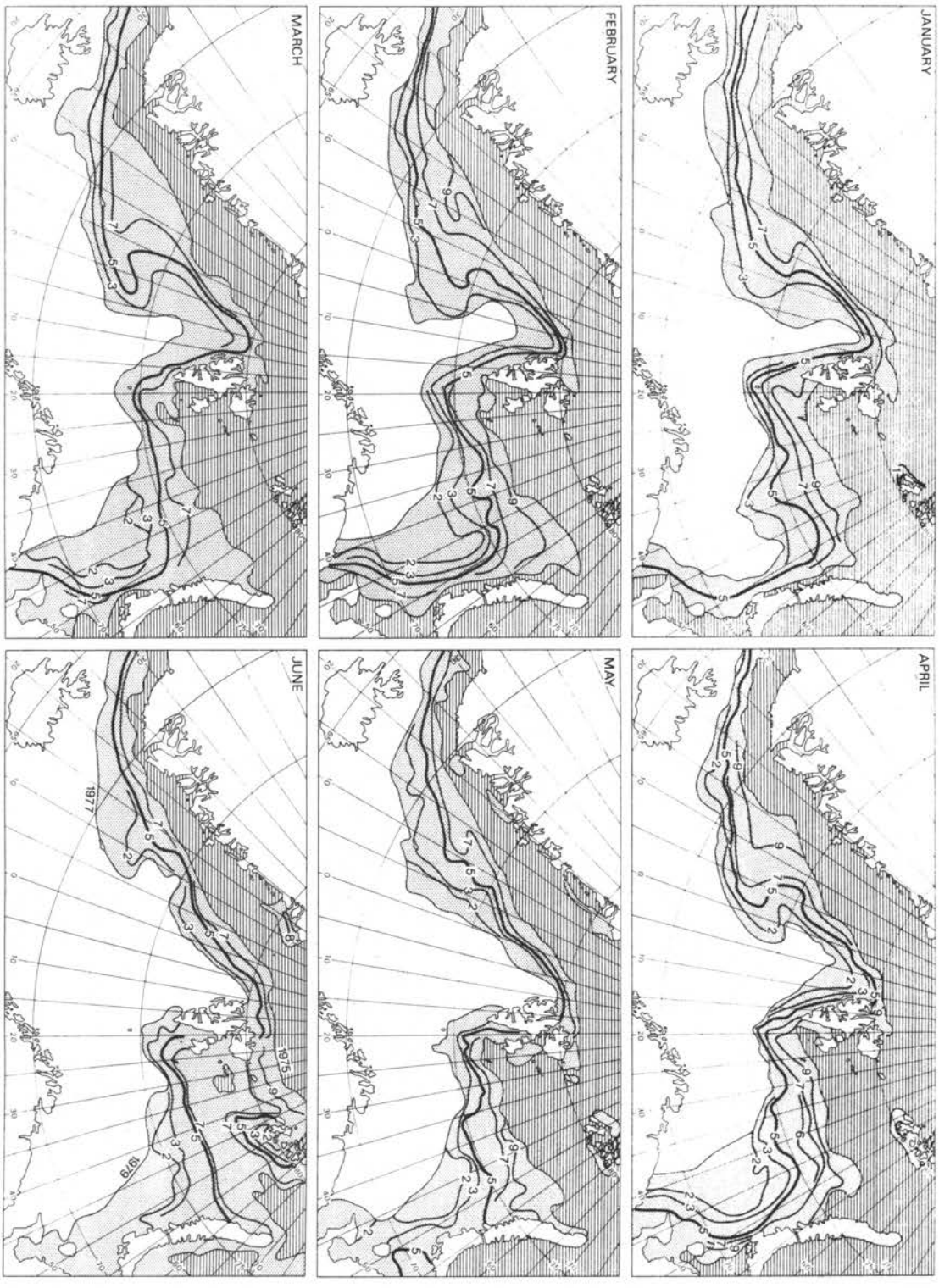

Fig. 5. Frequency distribution, given in tenths, of sea ice concentrations above 4/10 at the end of the month, 1971-1980.

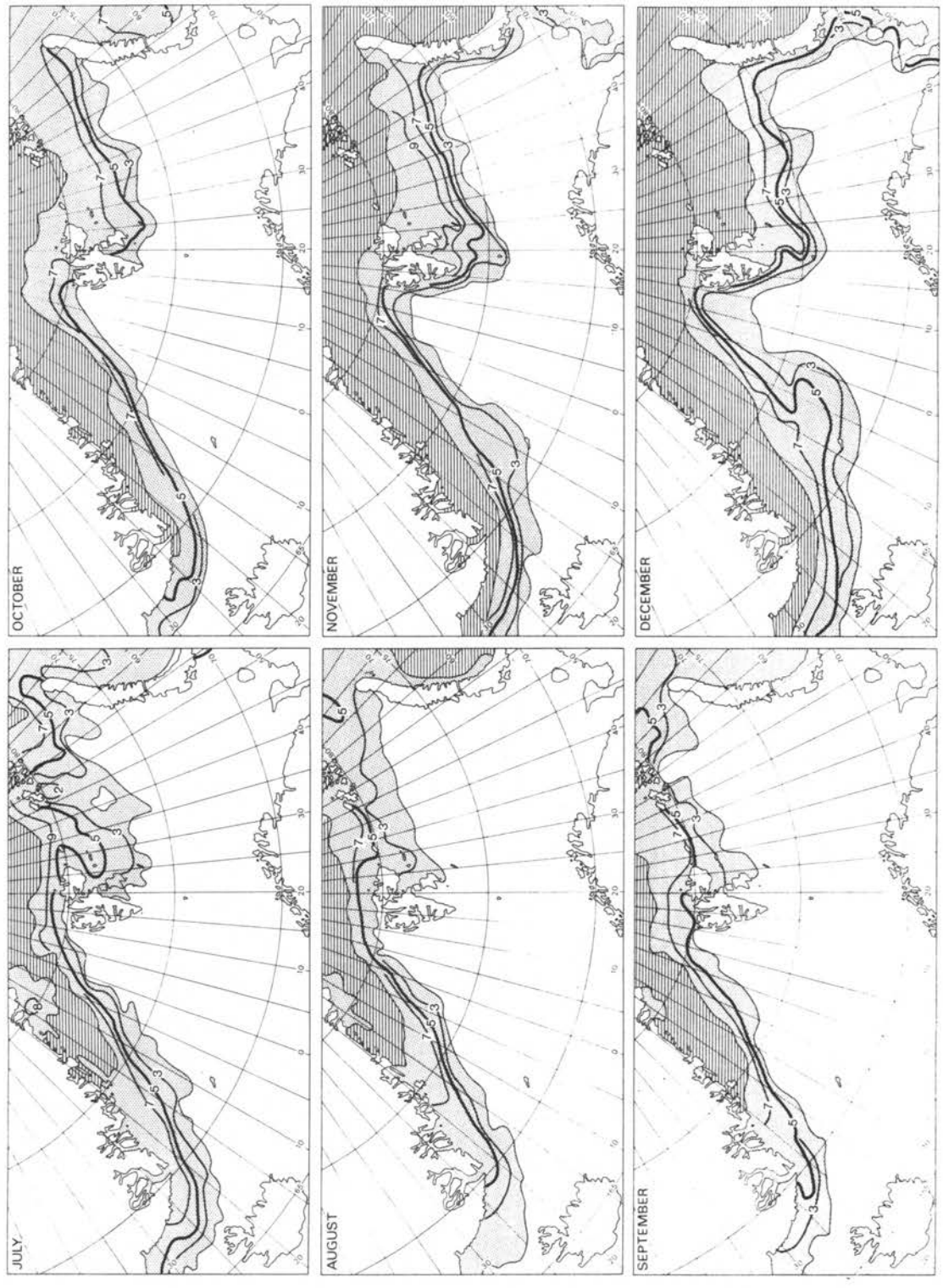

Fig. 5. Continued.....

an average less than 7/10 ice cover from the end of July to the end of September. According to old rules it is necessary to use ice-strengthened ships when the concentration becomes greater than 4/10. This means that one generally may have access with non-strengthened ships into areas south of 78°N in the eastern part of the Svalbard archipelago from the end of July through September. At 50°E the corresponding latitude is 80°N according to Walsh's data.

Results based on satellite information only give a more differentiated picture, as in Fig. 5 where the frequency distribution of the occurrence of sea ice concentrations $\geqslant$ 4/10 is given for the 1971-1980 period (Vinje 1981).

2.2. Special features

Special sea ice distributions are observed around islands, in straits or near the outer edge. Off-land winds will open up a flaw lead on the lee side after a very short duration (some hours), even during the cold season when the ice cover may be consolidated (Fig. 6).

The flaw lead may sometimes reach a width of several kilometres. When the wind turns, this lead will rapidly be closed and rafting and ridging may take place with varying intensity, dependent upon the wind strength and ocean current speed. Off-ice winds will cause a considerable divergence of the outer edge (Fig. 7) while on-ice winds will cause a convergence (Fig. 8) and we may at times get fairly high ridges near the outer edge ('havgard' in Norwegian) (Fig. 10). When the ice is forced through straits, a special fracture pattern is formed (Vinje 1977) (Fig. 11).

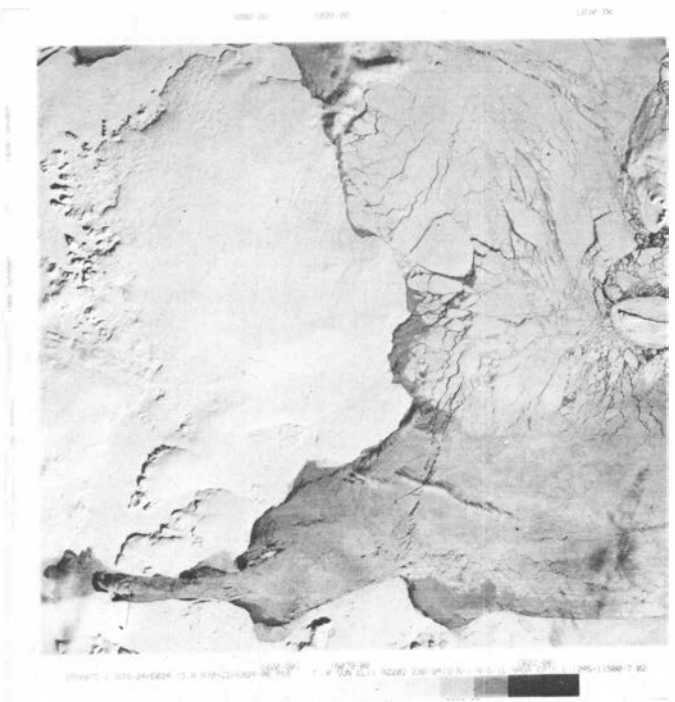

Fig. 6. Flaw lead along Nordaustlandet 25 March 1973 as shown on LANDSAT imagery. Frame: 185 km x 185 km.

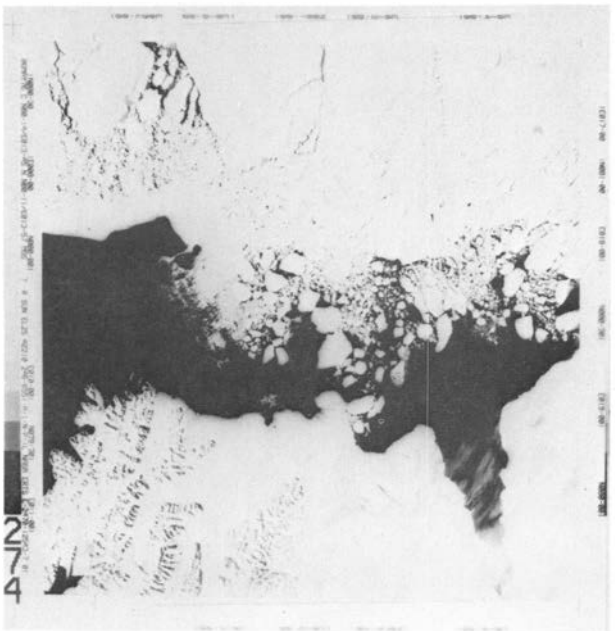

Fig. 7. Diffused ice edge caused by weak off-ice winds north of Svalbard. Note the well defined edge to the left where the strong West-Spitsbergen Current submerges the colder, lighter polar water. 6 May 1976. LANDSAT. Frame: 185 km x 185 km.

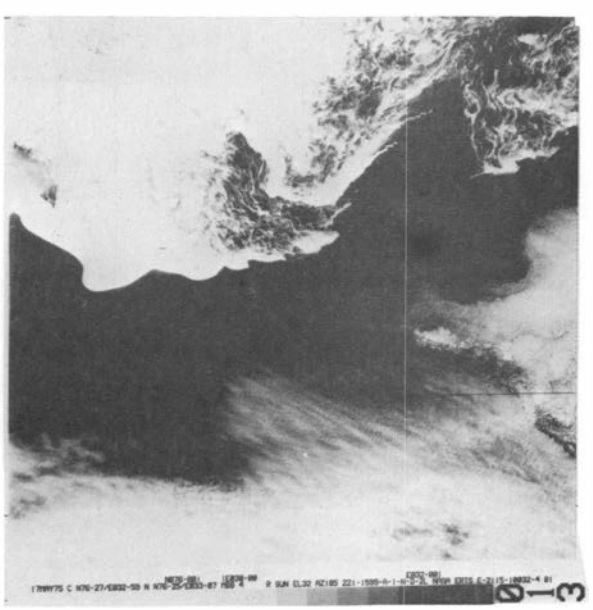

Fig. 8. Well defined ice edge during on-ice wind conditions (left hand side). Note the meandering trails in the upper area of the right hand side. Barents Sea 77.5°N - 33°E, 17 May, 1976. LANDSAT. Frame: 185 km x 185 km.

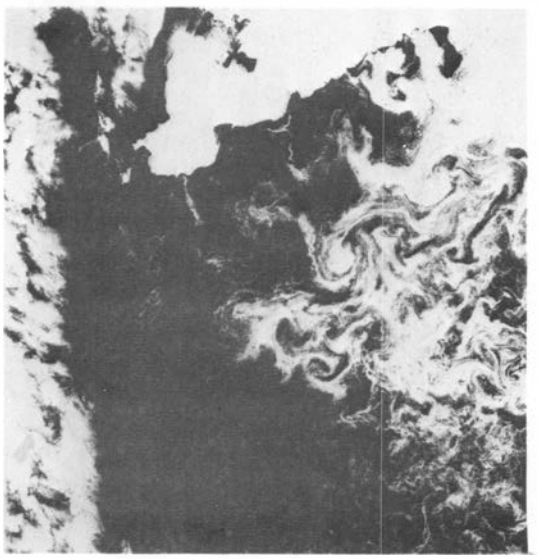

Fig. 9. A complex eddy pattern observed in scattered drift ice in Øst-Spitsbergenstrømmen during conditions with very weak westerly winds. 8 June 1976. LANDSAT. Frame: 185 km x 185 km.

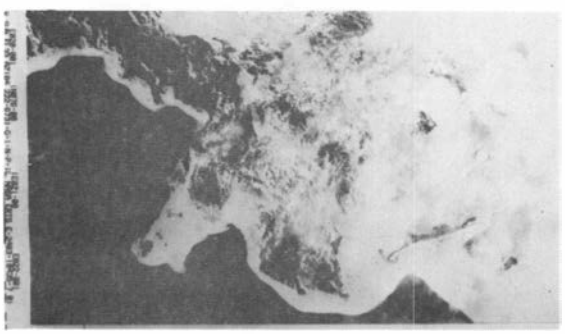

Fig. 10. A cold current branch protuding from the ice edge west of Hopen. On-ice wind conditions prevail after a period with ice-diverging off-ice winds. Note the foremost, well defined ice edge. 19 May 1976. LANDSAT. Frame width: 185 km.

When the wind is relatively weak, the surface ocean circulation may sometimes be clearly demonstrated by the distribution of sea ice. We may for instance see eddies (Fig. 9) or eddy trails (Fig. 8), embayments indicating effects of warm and cold neighbouring current branches (Fig. 10), or indications of upwelling processes (Fig. 11).

3. Morphology of sea ice fields in the Barents Sea

The complex composition of the drift ice in the Barents Sea suggests considerable variation in its morphology. The effects of low pressure systems are also more intense in the marginal areas of the Arctic than in the interior. When the wind stress abates, the sea ice will, on the other hand, be redistributed more freely in response to the imposed internal stresses. The vertical extension of the ridges during relaxation periods should therefore be less here than in the Arctic Ocean. This was indeed observed from a submarine transect from the Northern Greenland Sea into the Arctic Ocean (Wadhams et al. 1979).

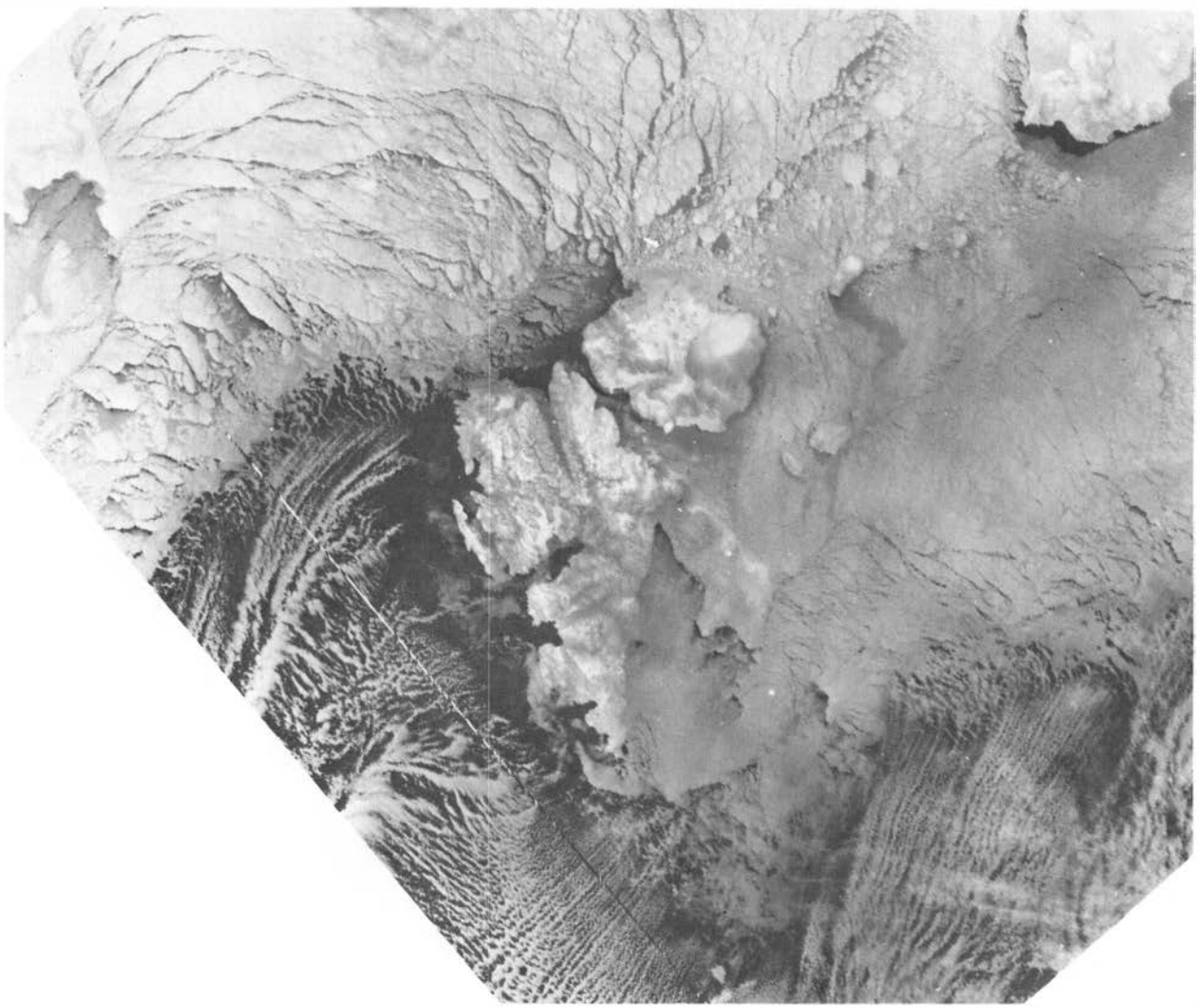

Fig. 11. Infra-red satellite imagery received at Tromsø Satellite Telemetry Station on 2 March 1981. Areas SW of Frans Josef Land and fjords of Spitsbergen are kept open probably because of upwelling processes. East to northeast winds of 10-15 kts prevail and the air temperature is between -36 and -28°C. Note the fracture pattern north of the Fram Strait with a dominance of parallelepiped-shaped floes.

3.1. Ridge density

The U.S. Naval Oceanographic Office (1962-69, 1971) has also made flights over the Barents Sea under the extensive Arctic sea ice observation programme 'Birds Eye'. The observations were made mostly over the eastern part of the Svalbard archipelago and the period covered was 1962-1971 (Fig. 17). The original observation data set gives altogether 169 countings during this period, of which 75% were over distances of 15 km, 14% over 10 km, and 11% over 5 km, approximately. The total number of ridges counted amounted to 2407. The seasonal frequency distribution of the ridge density (Fig. 12) shows that the most frequent densities increase from 1-4 ridges per kilometre during the winter season (November, December, Janu-

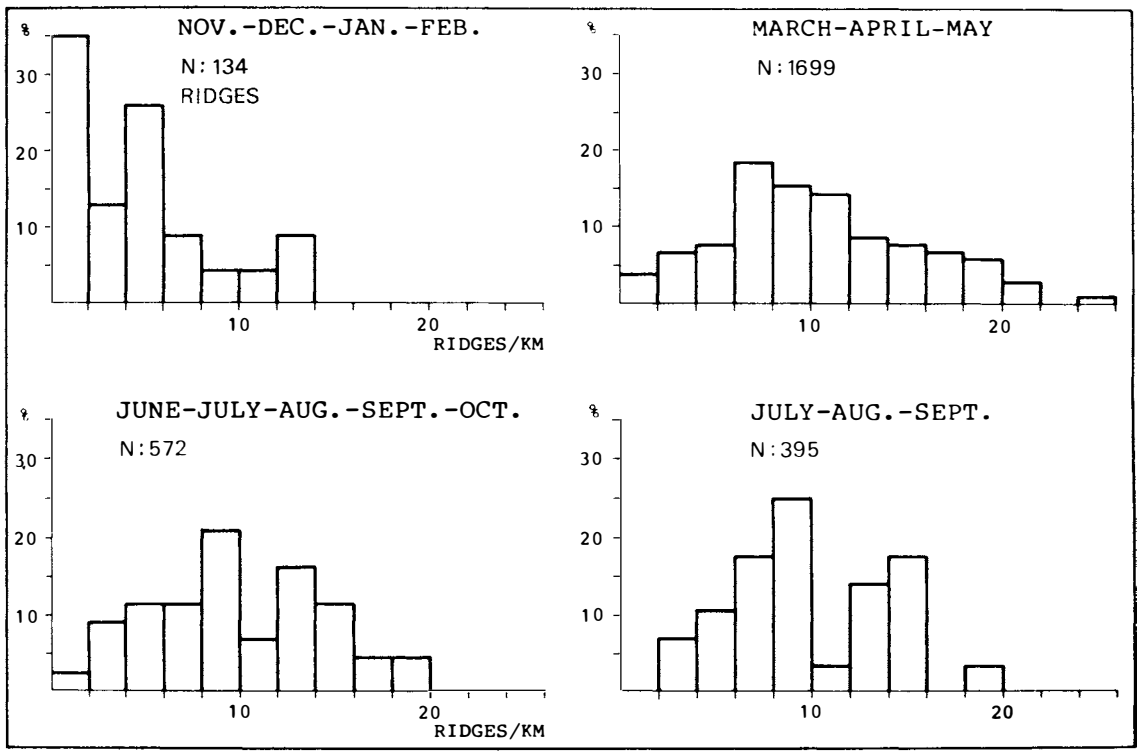

Fig. 12. Frequency distribution of ridge density (km^{-1}) for different seasons in the eastern part of the Svalbard archipelago (west of 35°E).

ary, and February) to about 9 ridges per kilometre during the disintegration period (June, July, August, September, and October). The widest distribution is observed during the transition period (March, April, and May) with the highest frequency at about 7 ridges per kilometre. During this period we also find the annual maximum of as much as 24 ridges per kilometre.

The seasonal density increase indicates an accumulation of ridges in the area. This seems reasonable as some of the ridges formed during the cold season should consolidate and be retained throughout the summer season. It is of interest to note that the observations obtained during the warm season (July, August, and September) indicate a bimodal density distribution with maximum frequencies around 9 and 15 ridges per kilometre. The lesser maximum presumably reflects the combined effect of the reduced resistance to ridging in melting ice and occasional wind induced increases in the concentration of old ice with consolidated ridges. (Most of the younger, unridged ice should have disintegrated by this time of the year.

Hibler et al. (1972) assumed spatially random occurrence of ridges and showed that the distribution of ridge spacings follows the exponential distribution. The exponential distribution was also found to fit the ridge spacings in the Gulf of Bothnia (Lappäranta 1981a). The density distribution east of Svalbard does not seem to follow any simple relationship, and for the

disintegration period the distribution seems even to be bimodal. The reason for the marked difference in distribution compared with other areas might be the more complex conditions east of Svalbard (with islands, strong tidal currents, and open boundaries) and/or different methods of observation. The ridge density in the 'Birds Eye' programme was determined by counting the ridges passing a reference mark on the observation port, mainly over a distance of 15 km, while Lappäranta's (1981a) results were obtained by a profilometer mounted on an ice-breaker. The difference in distribution will be scrutinized in the continued study of the data.

Lappäranta (1981a) found from observations that one ridge per kilometre accounts for 0.0221 m of equivalent level ice thickness. He reports on a ridge density of 9.7 km^{-1} which accordingly should give an equivalent level ice thickness of about 0.2 m (Lappäranta 1981b). This ridge density is about the same as found to be the most frequent one east of Svalbard. However, the ridge heights in the latter area should be greater than in the former one and the corresponding addition to the thickness of level ice should therefore here be greater than 0.2 m. Hibler et al. (1974) used the eq. $h_r=10\pi\mu h_s^2$, where h_r is the equivalent level ice thickness of ridged ice, μ is the ridge density and h_s the sail height. Assuming an average ridge height of 1 m, the equivalent level ice thickness with a ridge density of 9 km^{-1} should accordingly be 0.28 m, and this seems to be a more reasonable value for the Barents Sea.

The 'Birds Eye' observations (U.S. Naval Oceanographic Office 1962-1969, 1971) in the coastal area west of Spitsbergen have been treated separately. Apart from the transition season and the melting season, relatively few ridge countings have been made there (Fig. 17). The frequency distribution of the ridge density for the two mentioned seasons (Fig. 13), indicates narrower distribution range compared with Fig. 12 which represents the area east of Svalbard. In the western coastal areas the extreme density is only 12 km^{-1} which is half the maximum value observed to the east.

Fig. 14 shows the frequency distribution of ridge density between 35 and 45°E in the Barents Sea for the transition season. (The spatial and temporal 'Birds Eye' coverage east of 45°E (Fig. 17) is very poor and will

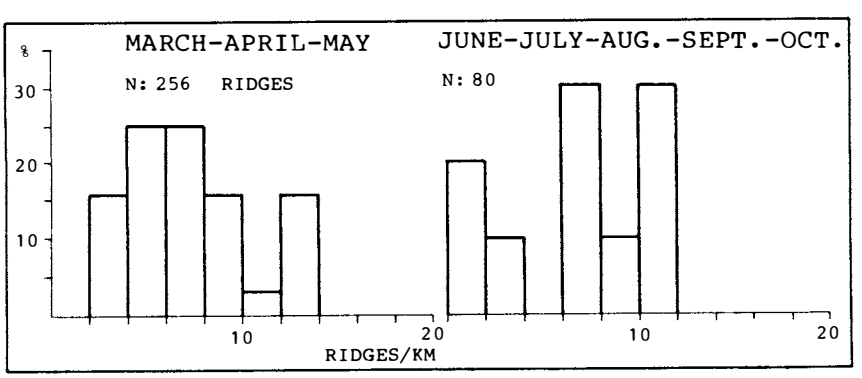

Fig. 13. Frequency distribution of ridge density (km^{-1}) in the coastal area west of Spitsbergen.

not be reproduced here). Also in this region (between 35 and 45°E) the distribution range is far narrower than further west. We find also a fairly high percentage (8%) at the extreme density (24 km^{-1}. The area in question is one of the first to open up during the disintegration season (cf. Fig. 5) indicating a predominance of relatively thin ice in this part of the Barents Sea. Thinner ice should be relatively less resistant to ridging forces and this might possibly explain the observed higher ridge density in this area, which is exposed to the same regional wind stress field.

3.2. Water openings

The observation of water openings was also a part of the 'Birds Eye' programme (U.S. Naval Oceanographic Office 1962-1969, 1971). Water openings were counted and measured along the flight track utilizing a reference mark on the observation port. Counts were made for 10-minute periods. The size of each opening was determined by multiplying the number of seconds elapsed for the reference mark to cross the opening by 100 metres/second, assuming an average ground speed of 180 knots. Water openings were then classified according to the following size categories:

1. Very small	< 50 m
2. Small	> 50 - 200 m
3. Medium	> 200 - 500 m
4. Large	$\geqslant 500$ m

Orientation relative to the aircraft heading was also recorded.

The frequenciy distribution of the widths of the 3805 water openings observed west of 35°E in the Barents Sea (Fig. 15) is of fairly similar shape for all seasons, with a uniform reduction in frequency towards the larger openings. The increased number of very small leads observed during the cold season in all probability reflects the effect of the rapid refreezing of openings which takes place at this time of the year.

The frequency distribution with respect to direction (Fig. 16) shows clearly that openings running in an easterly direction are the most predominant ones regardless of width and season. This seems reasonable, as

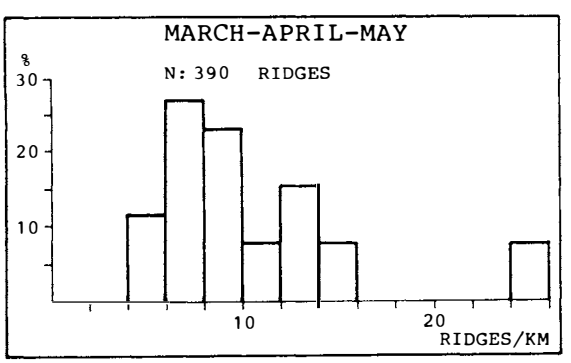

Fig. 14. Frequency distribution of ridge density (km^{-1}) between 35 and 45°E in the northern Barents Sea.

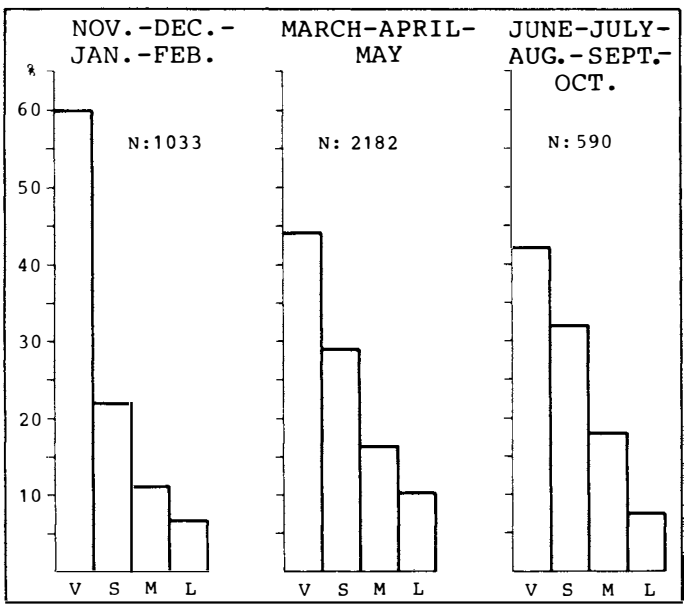

Fig. 15. Frequency distribution of widths of water openings in the eastern part of the Svalbard archipelago (west of 35°E). V: < 50 m, S: > 50-200 m, M: > 200-500 m, L: ⩾500 m.

water openings in the eastern part of the Svalbard archipelago are mostly formed in connection with diverging effects caused by northerly windds and/or by the southwestward directed ocean currents in this area. A secondary mode of random orientation is observed during the transition period. The reason for this is not clear.

The data base for water openings in the coastal area west of Spitsbergen is very sparse and the observations will therefore be omitted.

Altogether 484 water openings were observed in the area between 35 and 45°E in the Barents Sea. The frequency distributions of width and orientation (not reproduced here) are similar to those obtained for the area west of 35°E.

4. Morphology of sea ice fields in the Greenland Sea.

The Greenland Sea is more or less continuously supplied with drift ice from the Polar Ocean. The average drift speed through the passage between Greenland and Spitsbergen, the Fram Strait, has been observed to be about 9.5 cm s^{-1}. Considering the annual variation of the width of this ice flow over a period of years, we arrive at an average outflow of 1.08 mill km^2 $year^{-1}$ with mean possible maximum and minimum of 1.32 and 0.75 mill km^2 $year^{-1}$, respectively (Vinje 1982).

Divergence occurs more or less continuously in the drift ice once it has passed the constriction of the Fram Strait. During the cold season this results in the formation of large quantities of new ice. Based on the 'Birds Eye' data obtained during the first year of this programme, Wittman and Schule (1966) gave values of the percentage distribution of polar ice, thick winter- and new ice in the northern part of the Greenland Sea (Table 1).

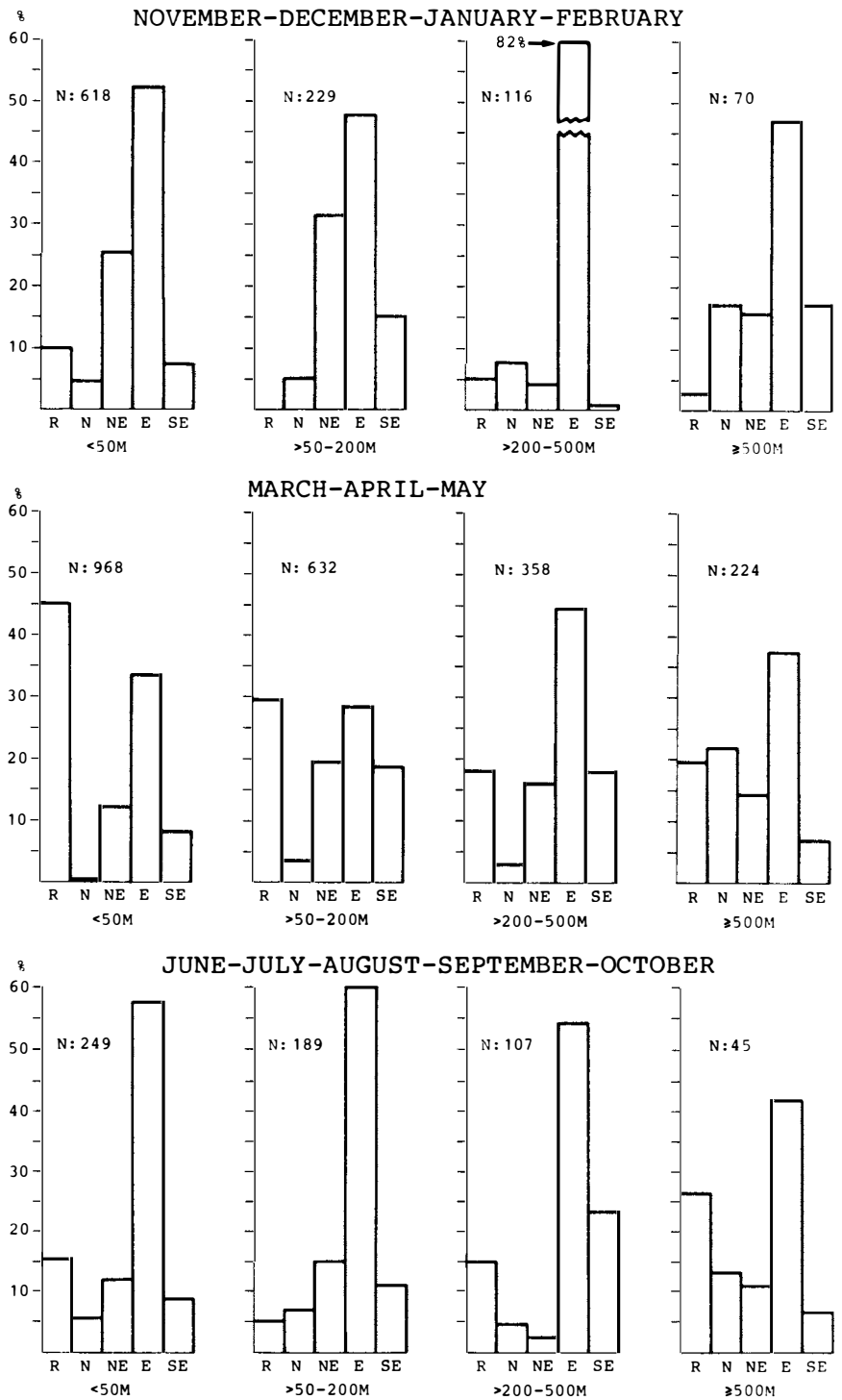

Fig. 16. Frequency distribution of orientation of water openings of various widths for three different seasons. Eastern part of the Svalbard archipelago (west of 35°E). Orientation: R = random, N = north, etc.

Table 1. - Relative percentage of the stage of development during various seasons for polar ice (P), thick winter ice (TW) and new ice (N) in the Greenland Sea (Wittman & Schule 1966).

	Jan-May	*Jun-Jul*	*Aug-Oct*	*Nov-Dec*
P	23	39	44	5
TW	47	34	31	43
N	30	27	26	52
Obs. number	128	35	99	90

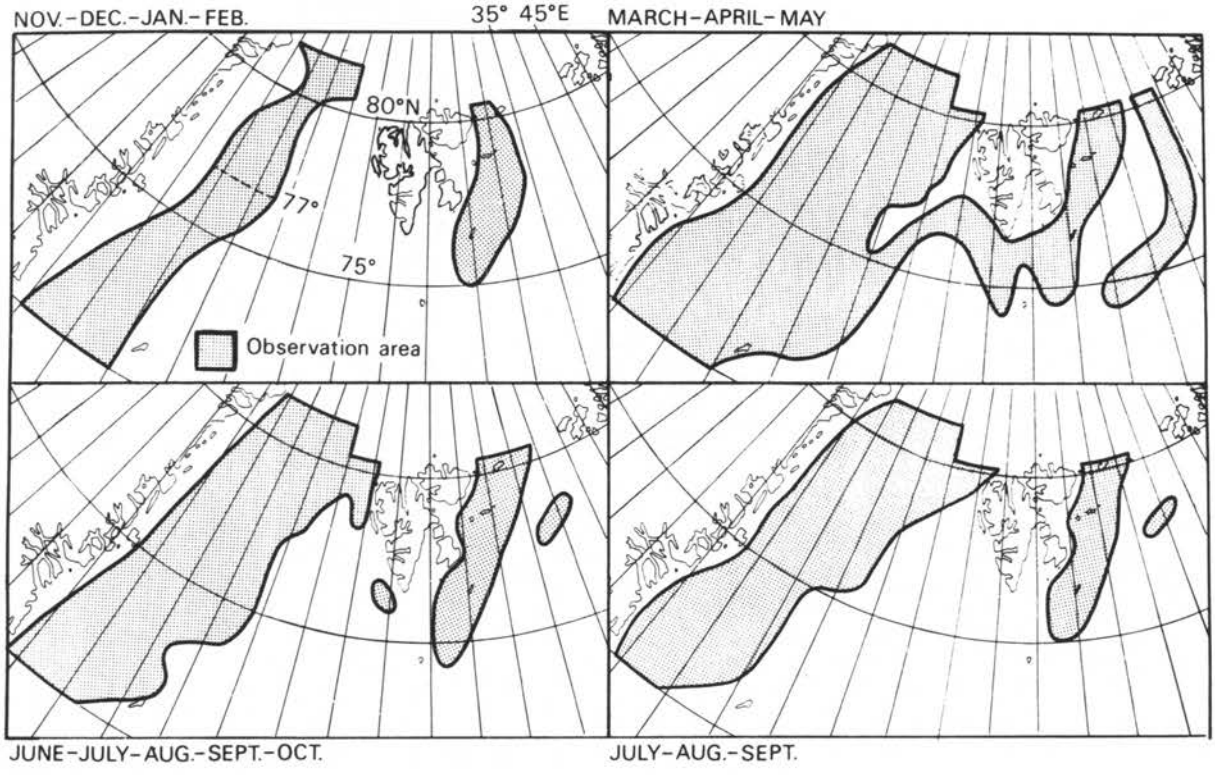

Fig. 17. Aerial coverage of the 'Birds Eye' flights for the various seasons.

We note the relative increase of polar ice as the melting proceeds through the summer and first part of the autumn. A drastic reduction occurs in the relative percentage of the polar ice in November - December because of the formation of new ice at this time of the year. The variation in the sea ice conditions may vary considerably from year to year, and the relative distribution of polar thick winter- and new ice may therefore show large year to year differences.

4.1. Ridge density

A series of 'Birds Eye' flights was undertaken over the Greenland Sea during the period 1962-1971 (U.S. Naval Oceanographic Office 1962-1969, 1971). The observations from the northern and southern part of the sea have been treated separately because of the anticipated difference in the sea ice conditions between the two regions (Fig. 17). The overflown areas varied from season to season in broad accordance with the corresponding extension of the ice fields.

4.1.1. Ridge density in the southern part of the Greenland Sea

Altogether 376 ridge countings were made, of which 62, 19, and 19% were performed over distances of about 15, 10, and 5 km, respectively. The total number of ridges counted was 4108.

The seasonal frequency distribution of ridge density (Fig. 18) shows that the most frequent density increases from about three ridges per kilometre during the winter season to seven ridges per kilometre in the spring season (March, April, May). This maximum frequency is somewhat lower than the one (9 km^{-1}) observed east of Svalbard. We note further that the absolute maximum density (19 km^{-1}) is also somewhat less than the one observed in the Barents Sea (25 km^{-1}). Such a difference might possibly be caused by the lesser resistance to ridging forces of the thinner ice in the Barents Sea, as well as an increased ridging effected by the islands in that area. A conclusive statement on the matter cannot be made as we do not know the corresponding wind and current stress fields of the two areas in question.

4.1.2. Ridge density in the northern part of the Greenland Sea

North of 77°N altogether 318 countings were carried out under the 'Birds Eye' programme in the Greenland Sea. Of these countings 69, 20, and 11% were made over distances of about 15, 10, and 5 km, respectively. The total number of ridges counted was 4581.

Apart from the spring season, the frequency distribution of ridge density in this part of the Greenland Sea (Fig. 18, upper part) shows distinctive characteristics when compared with the other areas discussed previously (Figs. 12, 13, 14, and 18, lower part). The most conspicuous feature is the very broad distribution during the summer and first part of the autumn. The percentage frequency of ridge density greater than 9 km^{-1} for June, July, and August is as high as 59%. East of Svalbard the corresponding figure is 41% and in the southern part of the Greenland Sea this percentage is as low as 32%. The high value (59%) in and south of the Fram Strait, seems reasonable as the exported ice from the Polar Ocean has passed through a constriction area. Some of this drift ice also comes from the maximum ridging area in the Polar Ocean which is north of Greenland (Wittman & Schule 1966). The marked southward decrease of ridge densities above 9 km^{-1} in the Greenland Sea clearly illustrates the effect of diverging as well as disintegrating processes as the ice drifts southwards in the East Greenland Current during the melting season.

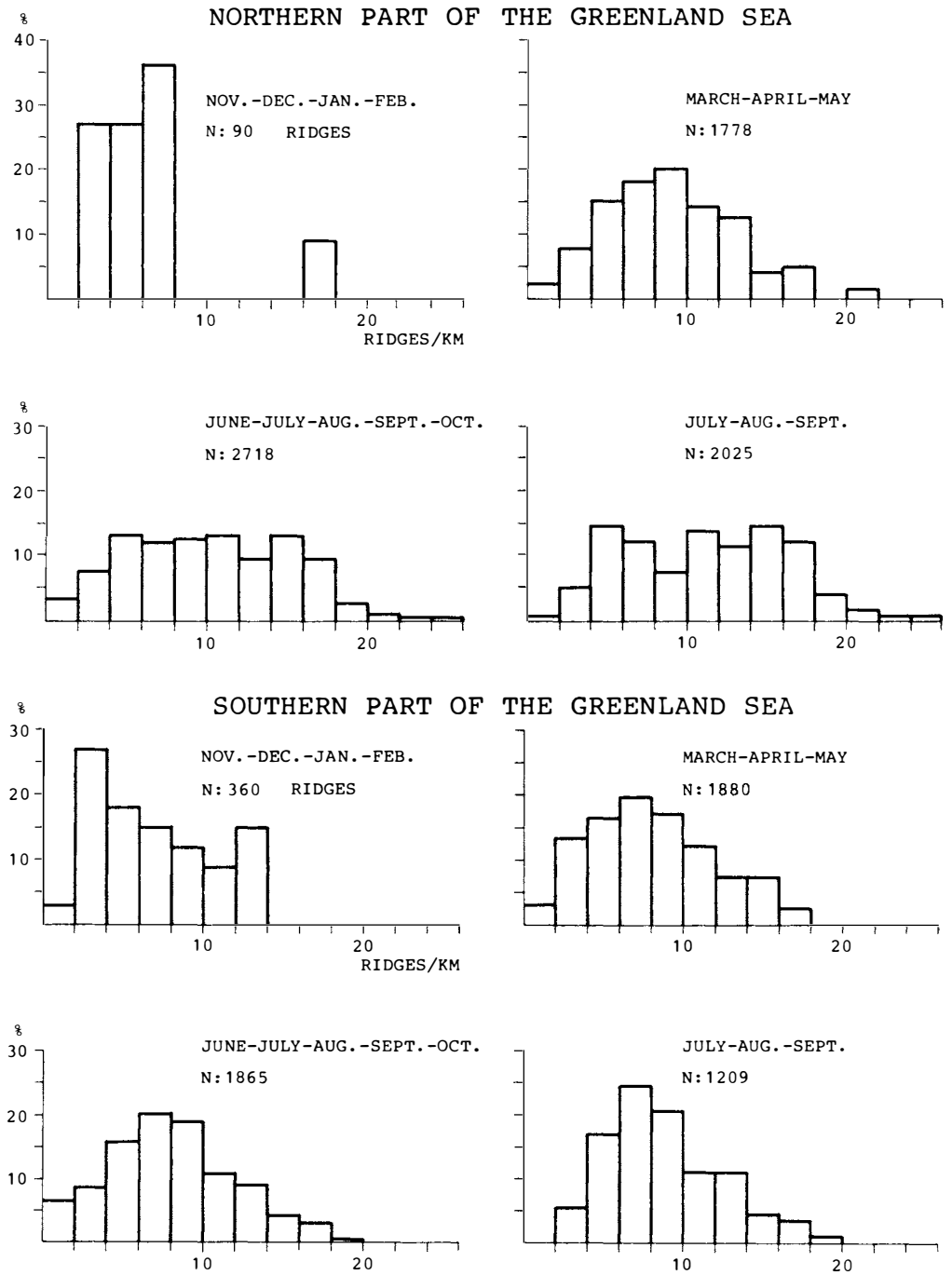

Fig. 18. Frequency distribution of ridge density (km^{-1}) for different seasons in the Greenland Sea. Upper part: north of 77°N. Lower part: south of 77°N.

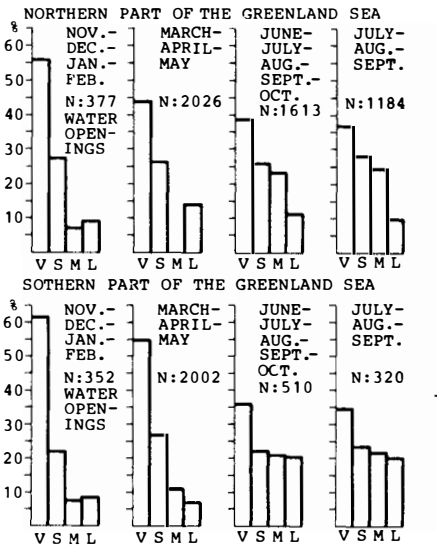

Fig. 19. Frequency distribution of widths of water openings in the Greenland Sea. V: < 50 m, S: > 50-200 m, M: < 200-500 m, L: ⩾ 500 m. Upper part: north of 77°N. Lower part: south of 77°N.

4.2. Water openings

4.2.1. Water openings in the southern part of the Greenland Sea

The classification of 2864 water openings was made on flights over the southern part of the Greenland Sea. The frequency of occurrence of water openings of various widths (Fig. 19, lower part) does not show the same uniform distribution as was found in the Barents Sea (Fig. 15). We see that the larger openings become markedly more frequent during the warmer season. This simply reflects the disintegration effects on the ice field in the area. The relatively high frequency of very small openings (less than 50 m) during the winter season reflects the current refreezing of water openings in a divergent ice field at that time of the year.

There is a marked difference in the frequency distribution for this area compared with the Barents Sea (Fig. 15), for the summer and first part of the autumn. This difference indicates that the ice fields are comparatively more divergent in the southern part of the Greenland Sea during this season.

The frequency distribution with respect to orientation for the southern part of the Greenland Sea (Fig. 20) shows a predominant occurrence of east-west running leads for all widths considered, as well as for all seasons. The orientation is, however, more broadly distributed in the spring season. During this time of the year the ice field has reached its maximum consolidation and the increased friction along the coast causes backward directed fractures along the friction border (Vinje & Finnekåsa unpublished). Because of the increase in speed with distance from the coast in the East Greenland Current, these leads will open up and further east will get a more easterly orientation. It might be that this effect could to some extent explain the broader distribution of orientation for the spring season in this area.

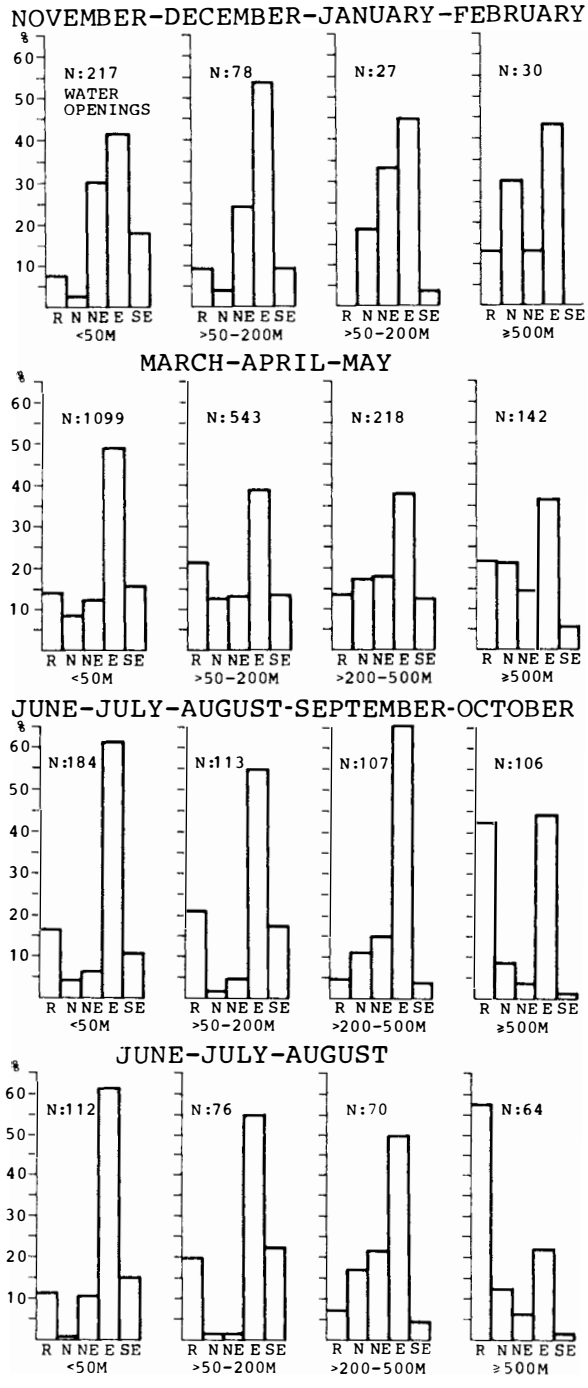

Fig. 20. Seasonal frequency distribution of orientation of water openings of various widths south of 77°N in the Greenland Sea. R = random, N = north, etc.

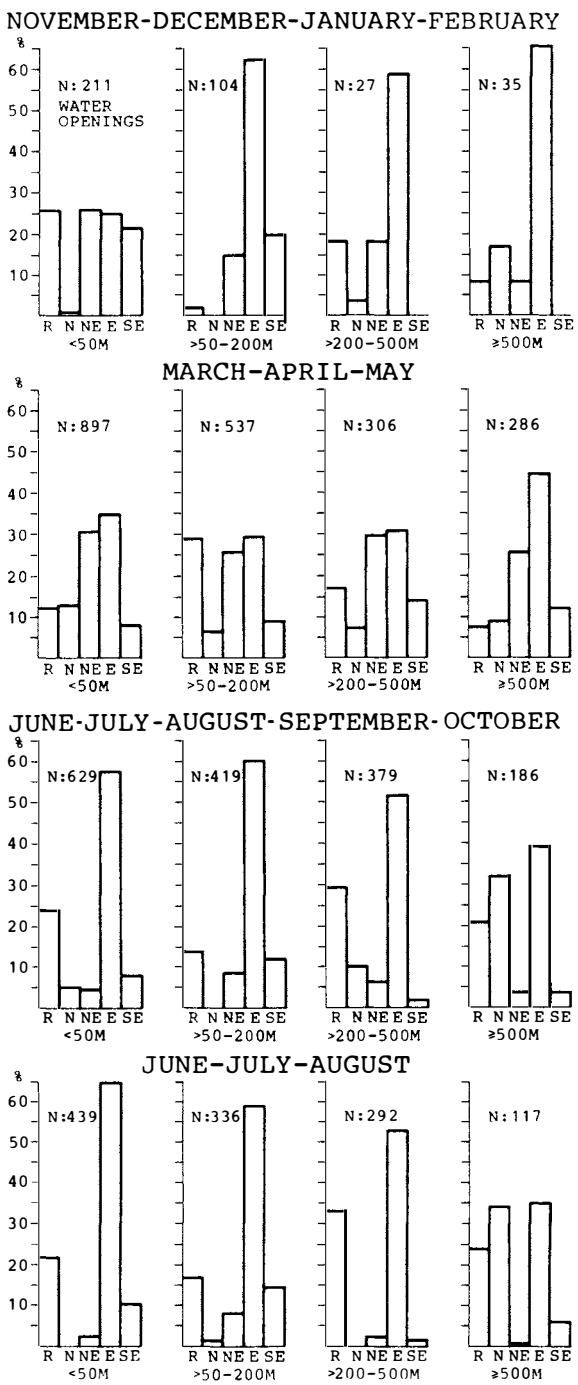

Fig. 21. Seasonal frequency distribution of orientation of water openings of various widths north of 77°N in the Greenland Sea. R = random, N = north, etc.

4.2.2. Water openings in the northern part of the Greenland Sea

The classification of altogether 4016 water openings was made on flights over the northern part of the Greenland Sea. Also for this area, the frequency of occurrence of water openings of various widths (Fig. 19, upper part) does not show such a uniform distribution as was found in the Barents Sea for all seasons (Fig. 15).

A broad similarity is seen in the frequency distribution from season to season in both parts of the Greenland Sea (Fig. 19). However, during the summer and first part of the autumn, the largest openings are markedly less frequent in the north. This difference probably reflects the effect of convergence in the ice field due to its relatively recent passage through the Fram Strait. An opposite condition, however, is seen to exist during the spring period. At this time of the year, large-scale freezing may still go on, and it will obviously take some time before the openings refreeze in the divergent flow to the south of the Fram Strait.

The frequency distribution of the orientation of the water openings in the northern part of the Greenland Sea (Fig. 21) shows a somewhat different picture compared with the one observed in the southern part (Fig. 20). An easterly orientation is very predominant in most of the graphs. Other graphs, and in particular those of the spring season, reveal a more dispersed distribution. We have maximum consolidation of the ice field during the spring season, and a special fracture pattern may then be observed when drift ice is forced through passages. Arching effects are indicated by numerous U-shaped leads running across the passage, and a great number of floes with a parallel epipedian shape is then formed north of, and in the passage (Fig. 11). The special distribution of orientation, observed south of the Fram Strait, might therefore possibly be explained by this special fracturing effect. Arching effects in ice flow through straits have been mathematically treated by Pritchard et al. (1979).

Acknowledgements

This report was prepared under a contract with a series of Norwegian industrial sponsors in the joint research project 'Marine Structures and Ships in Ice'.

The 'Birds Eye' observations and the digitized 25-year data set on sea ice distribution were kindly made available by the U.S. Naval Oceanographic Office and the U.S. National Center of Atmospheric Research, respectively.

References

Hibler, W. D. III, Weeks, W. F. & Mock, S. J. 1972: Statistical aspects of sea ice ridge distribution. *Jour. Geoph. Res. 77(30).*

Hibler, W. D. III, Mock, S. J. & Tucker, W. B. III 1974: Classification and variation of sea ice ridging in the Western Arctic Basin. *Jour. Geoph. Res. 79(18).*

Lappäranta, M. 1981a: Statistical features of sea ice ridging in the Gulf of Bothnia. *Forskningsrapport 32*, Styrelsen för Vintersjöfartsforskning.

Lappäranta, M. 1981b: On the structure and mechanics of pack ice in the Bothnian Bay. *Finnish Marine Res, 248.* Helsinki.

Loeng, H. & Vinje, T. E. 1979: On the sea-ice conditions in the Greenland and Barents Seas. *POAC 79, Vol. I.* NTH, Trondheim.

Pritchard, R. S., Reimer, R. W. & Coon, M. D. 1979: Ice flow through straits. *POAC 79, Vol. III.* NTH, Trondheim.

U. S. Naval Oceanographic Office, 1962-1969 and 1971: *'Birds Eye' informal reports. Nos: 1-8 (1962), 1-8 (1963), 1-9 (1964), 1-11 (1965), 1-7 (1966), 1-4 (1967), 1-12 (1968), 1-3 and 6-7 (1969), and 4-10 (1971).* (Not published.)

Vinje, T. E. 1976: Sea ice conditions in the European sector of the marginal seas of the Arctic, 1966-1975. *Nor. Polarinst. Årbok 1975.*

Vinje, T. E. 1977: Sea ice studies in the Spitsbergen - Greenland area. *LANDSAT Rept. E77-10206. US Dept. of Commerce.* Natl. Tech Info Service, Springfield, Va.

Vinje, T. E. 1981: Frequency distribution of sea ice in the Greenland and Barents Seas, 1971-1980. *Nor. Polarinst. Årbok 1980.*

Vinje, T. E. 1982: The drift pattern of sea ice in the Arctic with particular reference to the Atlantic approach. In L. Rey (ed.): *The Arctic Ocean: Environmental Problems of the Polar Mediterranean.* McMillan Publishers Ltd. London.

Wadhams, P., Gill, A. E. & Linden, P. F. 1979: Transects by submarine of the East Greenland Polar Front. *Deep Sea Res. 26*: 1311-1327.

Wittman, W. J. & Schule, J. J. 1966: Comments on the mass budget of Arctic pack ice. *Proc. of the Symp. on the Arctic Heat Budget and Atmos. Circ.* The Rand Corporation, Santa Monica.